Kinetic model for the long term stability of contaminated monoatomic nanowires

P. Vélez,[1] S. A. Dassie,[1,2] and E. P. M. Leiva[1,*]

[1]*Departamento de Matemática y Física–INFIQC, Facultad de Ciencias Químicas, Universidad Nacional de Córdoba, Ciudad Universitaria, X5000HUA Córdoba, Argentina*

[2]*Departamento de Fisicoquímica–INFIQC, Facultad de Ciencias Químicas, Universidad Nacional de Córdoba, Ciudad Universitaria, X5000HUA Córdoba, Argentina*

(Received 2 December 2009; revised manuscript received 28 January 2010; published 29 March 2010)

The kinetic behavior of pure Au nanowires upon rupture is analyzed in comparison with that of nanowires contaminated with H and C. The latter present larger activation energies for the rupture for all elongations and as a consequence these contaminated wires are predicted to live longer, as observed experimentally. The kinetic analysis is complemented by an analysis in terms of the concept of reaction force. It is found that this is the relevant quantity to analyze when considering the stability of the nanowires in the limit of low elongations rates or relatively high temperatures rather than the longitudinal force acting on the nanowire. The elastic and electronic contributions to the rupture process are obtained for each system. While the latter are similar in all cases, the elastic part is found to play the decisive role to make the difference. The present results suggest that measurement of the force constant of the junction may help to determine the chemical nature of the impurity.

DOI: 10.1103/PhysRevB.81.125440 PACS number(s): 73.63.Rt, 73.63.Nm, 73.63.Bd, 73.21.Hb

I. INTRODUCTION

Numerous experiments show that the lifetime of a Au monoatomic nanowire (NW) is of the order of a second, presenting surprisingly large Au-Au distances in comparison with (i) the equilibrium distance of a Au diatomic molecule (2.5 Å), (ii) the nearest-neighbor distance of Au atoms in the fcc structure (2.88 Å), and (iii) the Au-Au distance observed in a Au monoatomic NW just before rupture, as obtained from first-principles calculations[1–12] and molecular dynamics using semiempirical interaction potentials[6,13,14] (2.9–3.0 Å). The images of Au monoatomic chains that show long distances (3.6–4 Å) were obtained in numerous experiments using transmission electron microscopy (TEM) and high-resolution transmission electron microscopy (HRTEM), employing the technique of electron beam lithography for their generation.[15–20] Similarly, Yanson *et al.*[21] determined Au-Au separation distances of 3.6 Å from chain-length histograms using the method of mechanically controlled break junction (MCBJ). However, it must be pointed out that not all experiments show anomalous Au-Au distances. In particular, Takai *et al.*[22] have reported the existence of very stable Au monoatomic NWs with Au-Au distances very close to those of the bulk metal (~2.9 Å).

The most widespread hypothesis to explain the occurrence of the long Au-Au distances observed experimentally has been the presence of atomic impurities (C, H, O, and S) intercalated between the Au atoms. This type of conjecture has only been tested by means of computational tools using first-principles methods, since these light atoms cannot be visualized by electron microscopy techniques due to the low contrast they present in comparison with the heavier Au atoms. The contaminants in the Au chains could be due to the presence of residual gases in the vacuum chamber of the TEM. In this respect, hydrogen[23] and oxygen[4] are impurities very difficult to eliminate, even under ultrahigh vacuum (UHV) conditions. On the other hand, carbon is the impurity most frequently found in bulk Au.[16] It must be also pointed out that some authors deny of possibility of hydrogen contamination,[24] using as an argument that the intensity of the current used in the electron beam lithography experiments (30–100 A/cm^2) is high enough to clean the region irradiated from the light elements.

Legoas *et al.*[16] have tackled the problem of the formation of long Au chains from both experimental and theoretical viewpoints, trying to understand the existence of the anomalous Au-Au distances. They considered especially the case of carbon as contaminant. From the results of the experiments, these authors obtained histograms showing a continuous distributions of Au-Au separation distances between 2.88 and 3.7 Å, and an isolated peak at the extremely large value of 4.8 Å, similar to that found by Koizumi *et al.*[25] In order to understand the unusually large Au-Au distances observed, the authors of Ref. 16 modeled the gold monoatomic chains, in the *naked* cluster approach, by means of geometry optimization of an isolated linear chain without the application of stress to the system. These calculations were performed within the framework of density-functional theory, using the local density approximation for the exchange correlation energy functional. The results of these simulations show that the large Au-Au distances (4–5 Å) could be due to the presence of impurities consisting of two consecutive carbon atoms (C_2), while the distribution of distances between 3 and 3.7 Å would be the consequence of the occurrence of a mixing of Au-Au bonds with the contamination of single carbon atoms. On the other hand, Skorodumova and Simak,[5] also used first-principles calculations to support the hypothesis that the unusual stability of Au NWs could be explained by the presence of hydrogen atoms, which would be able to stabilize the structures observed experimentally. In their simulations, these authors found that upon stretching, the monatomic chain turns to be linear, with Au-Au distance of 3.8 Å just before rupture. The cohesive energy for the contaminated wire was found two times lower than that of the pure one. This latter effect was attributed to the partial charge transfer of Au toward hydrogen with the concomitant strengthening of the NW bonds.

A further analysis of the possible candidates as contaminants present in the Au NWs was performed by Novaes *et al.*,[26] also from first-principles calculations. They studied the

influence of H, B, C, N, O, and S on the structural and electronic properties of a Au NW. They proposed different explanations for each of the peaks observed in the histograms of Fig. 3 in Ref. 16. In the case of the peak at 3.0–3.1 Å, they proposed that it could be due to pure or contaminated NWs. The second peak (3.5–3.6 Å) was definitely attributed to the presence of impurities, where hydrogen was the best candidate. Finally, the peak at large distances (4.8 Å) was attributed to S as contaminant.

In summary, the discussion on which are the impurities that really would explain the unusually long Au-Au distances can be followed in numerous articles.[4,16,24,26–34] However, most of these theoretical approximations only involve geometry optimization of infinite Au chains (without the effect of the connecting electrodes)[4,16,26,27,32] or first-principles atom dynamics simulations of a few nanoseconds, or under extremely large elongation rates, as compared with the experimental ones.[24,30,31] Thus, a challenging topic appears: the simulation of NW rupture in the time scale of the seconds when the system is contaminated with atomic impurities. This is an important issue, since such an implementation would allow the calculation of energetic, mechanical, and electronic properties in a situation close to the experimental conditions.

In order to analyze the lifetime of a pure Au nanowire, we proposed in a previous work[35] a kinetic model to study the stability of monoatomic NWs based on transition state theory. The model used to describe a monoatomic Au nanojunction, was an infinite chain of Au atoms generated from a supercell containing four atoms, with the finding that pure Au monoatomic NWs should not present Au-Au interatomic distances larger than 2.66 Å at room temperature. In the present work we develop a comparative computational study of the energetic, structural, and kinetic properties of pure and contaminated Au NWs, with H and C as impurities under stress, making predictions for the lifetime of these NWs in a wide time scale, compatible with the experimental one. We apply an extension of the model presented previously to study the stability of pure Au NWs,[35] and further analyze the reaction coordinate in terms of the concept of the "reaction force" as developed by Toro Labbé and co-workers.[36,37] This will be found a useful tool to understand the dynamics of these systems.

II. CALCULATION MODEL

Figure 1 shows a scheme of the unit cell employed to simulate the pure and contaminated Au NWs considered here. The gray circles represent Au atoms, which remain fixed at their positions during the relaxation processes. The latter consists in a local energy minimization procedure by means of the conjugate gradient method or a search of a minimum energy path (MEP) by means of the nudged elastic band method (NEB).[38,39] In this method, a discrete number of structures (called images) are placed along the guessed MEP. These images are moved according to: (A) the force acting on them perpendicular to the path and (B) an artificial spring force keeping the images spaced along the MEP. The highest-energy image gives a good estimate of the transition state.

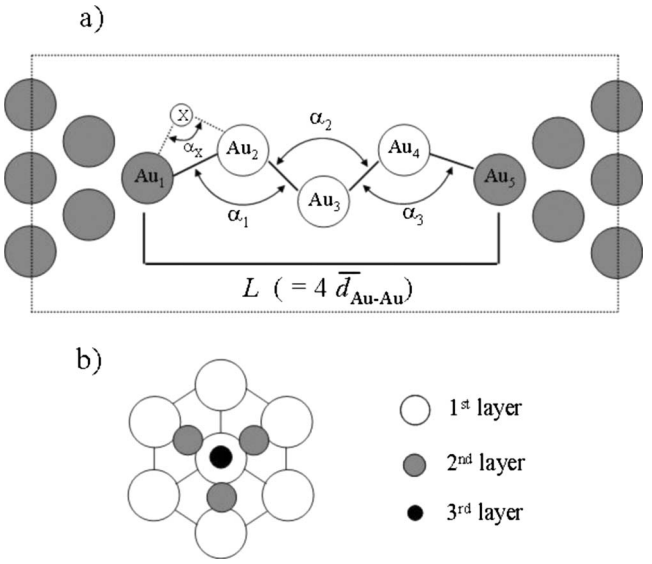

FIG. 1. Schematic representation of the unit cell employed in the present calculations (a) the rectangle indicates the extension of the unit cell. The gray circles represent the Au atoms fixed during the simulation. α_1, α_2, and α_3 are the bond angles between the Au atoms and α_X is the angle defined by the atoms Au_1-X-Au_2, where *X* represents the atomic impurity, in the present case H or C. *L* is the total chain length and $\bar{d}_{\text{Au-Au}}$ is the average Au-Au separation distance. (b) Front view of the pyramid of Au atoms shown in (a).

The energy along the MEP is usually given as a function of a "reaction coordinate" (RC), which is a one dimensional coordinate that represents the progress along the MEP.

In mathematical terms, we have defined here a normalized reaction coordinate (NRC) at image $N+1$ of the NEB chain as

$$\text{NRC} = \frac{\sqrt{\sum_{j=1}^{N} |\Delta \mathbf{l_j}|^2}}{\sum_{j=1}^{N_{tot}} |\Delta \mathbf{l_j}|^2}, \tag{1}$$

where $\Delta \mathbf{l_j}$ is the vector joining images j and $j+1$ and N_{tot} is the total number of images of the chain.

In the case of contaminated NWs the circle marked with an *X* represents the location of a H or a C atom. This figure also shows the definition of the α_1, α_2, and α_3 bond angles, determined by the atoms relevant for the analysis of the rupture of the NW.

The length of the NW and *L*, is defined here as the distance between the atoms Au_1 and Au_5. We also define an average Au-Au separation, $\bar{d}_{\text{Au-Au}}$, as $\bar{d}_{\text{Au-Au}}=L/4$. Figure 1(b) shows the front view of one of the pyramid of Au atoms, represented as gray circles in Fig. 1(a). The present systems contains as a whole 18 atoms. It must be emphasized that in the case of calculations for pure Au NWs, the present systems deliver results that are close to calculations performed with only four atoms in the unit cell.[5,16] This indicates that the mechanical properties of NWs appear to be quite local, with a rather slight dependence from the bulky atomic envi-

ronment. The atomic impurity was located between the atoms Au_1 and Au_2. We made this choice because in the literature we found first-principles calculations, similar to those performed here, where the H and C were positioned at a similar place, as well as between the Au_2 and Au_3 atoms, with similar results.[26,32] As we will find below, the present results agree with those where the impurity was located at another sites of the chain. The electronic structure calculations were performed with the SIESTA code.[40–44] The unit cell presented in Fig. 1 was oriented along the z axis, using periodic boundary conditions. The basis set for the valence electrons was a double-ζ polarized one. The number of k points for the z direction was changed until obtaining a convergence in the energy of the system better than 0.002 eV/atom. This resulted in a $1\times1\times30$ k-point grid. The separation between neighboring chains in the x-y direction was 20 Å to ensure convergence in the energy of the systems. The exchange and correlation effects were described within the generalized gradient approximation using the Perdew-Burke-Ernzerhof functional.[45] The stretching of the NW was simulated by increasing the size of the supercell in the z direction in 0.1 Å steps.

III. RESULTS AND DISCUSSION

A. Structure and energetics of pure and contaminated Au NWs

In a first approach, we consider the energy and stability of monatomic Au pure and H- or C-contaminated Au NWs under stress. This was achieved by stretching the wire as described in Sec. II. The top of Fig. 2 shows the energy curves of the pure Au system (Au-p) as a function of the average Au-Au distance $\bar{d}_{\text{Au-Au}}$. Similar curves are reported there for the hydrogen (Au-H, middle), and carbon (Au-C, bottom) contaminated systems.

For all the systems we shall refer to the "equilibrium" state as that where the derivative of the energy with respect to the elongation is equal to zero. This corresponds to a minimum in the case of the Au-p and Au-C NWs, or to an inflection point in the case of the Au-H at $\bar{d}_{\text{Au-Au}}=2.375$ Å (see Fig. 2). In both Au-H and Au-C the decreasing energy at lower elongations is an indication of a deeper minimum when the system is compressed. The reason for this is the formation of a more compact structure under these conditions. The rupture force will be considered to be that value of the force F_z where it presents a maximum at long elongations, being the force defined as[6,12,26,27,35,46,47]

$$F_z = -\frac{\partial}{\partial \Delta z} E(\Delta z), \tag{2}$$

where Δz is the elongation of the NW. Δz is defined as $\Delta z = L - L_0$, where L_0 is the chain length at equilibrium for each system. Accordingly, we refer in the following to the "at rupture" state, meaning that where the coordinates of the atoms are such that $\frac{\partial F_z}{\partial \Delta z}=0$ (maximum force). With this definition, we are trying to address the status of the system just at the point where the NW is breaking by further force application.

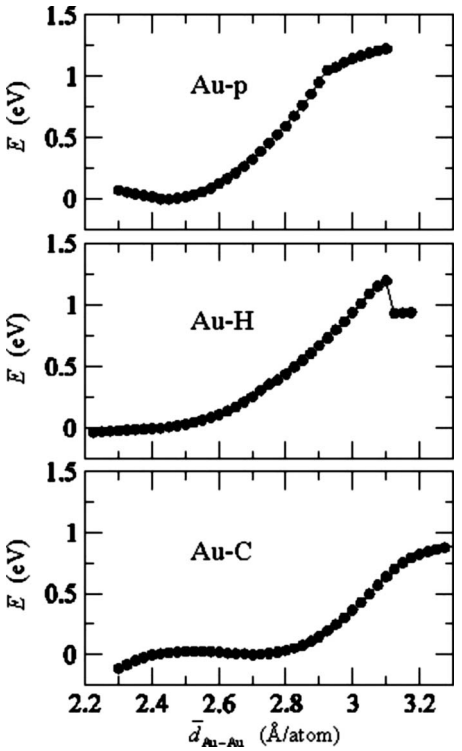

FIG. 2. System relative energy, E, for the pure Au NW of Fig. 1 (Au-p, top) and for a similar nanowire contaminated with hydrogen (Au-H, middle), and carbon (Au-C, bottom), as a function of the average Au-Au distance $\bar{d}_{\text{Au-Au}}$.

The structural information at the equilibrium and at rupture states of the NWs are shown in Tables I and II, respectively, for the three system types considered.

Considering the length difference between the at rupture and equilibrium states of the different systems, we find that the stretching lengths of the Au-p and Au-C systems are 1.9 and 1.6 Å, respectively, while the elongation of the Au-H system is considerably larger (2.6 Å). This fact bears direct

TABLE I. Structural information of the pure NW (Au-p) and contaminated with hydrogen (Au-H) or carbon (Au-C) at the equilibrium situation. The $d(1,2)$ bond distance and the α_X bond angle of the impurity are in boldface.

	Au-p	Au-H	Au-C
L_e (Å)	9.80	9.60	10.8
d(1,2) (Å)	2.63	**2.76**	**3.78**
d(2,3) (Å)	2.64	2.62	2.59
d(3,4) (Å)	2.63	2.67	2.66
d(4,5) (Å)	2.63	2.61	2.62
α_1 (°)	139.5	149.6	161.8
α_2 (°)	125.2	108.6	116.5
α_3 (°)	139.7	157.4	136.0
α_X (°)	---	**102.5**	**168.5**

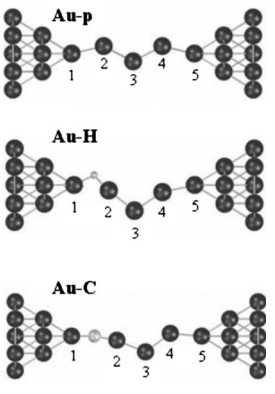

TABLE II. Structural information of the pure Au (Au-p) and hydrogen (Au-H) or carbon contaminated (Au-C) NWs close to rupture. The arrows show the bond at which the NW breaks. The $d(1,2)$ bond distance and the α_X bond angle of the impurity are in boldface.

	Au-p	Au-H	Au-C
L^* (Å)	11.7	12.2	12.4
d(1,2) (Å)	2.85	**3.58**	**3.87**
d(2,3) (Å)	2.95	2.75	2.67
d(3,4) (Å)	3.05	3.16	3.15
d(4,5) (Å)	2.85	2.71	2.71
α_1 (°)	179.3	178.6	178.5
α_2 (°)	179.7	177.0	176.5
α_3 (°)	179.9	178.5	178.2
α_X (°)	---	**179.2**	**179.5**

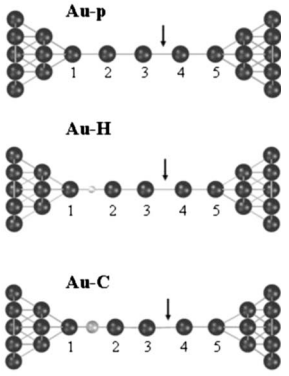

consequences for the force constant k_z, as we will see later on. From Table I we find that the equilibrium geometries of the contaminated systems are very different from each other. Close to equilibrium, the presence of the H atom changes only slightly the $d(1,2)$ bond distance, while the carbon atom inserts itself almost completely in the middle of this bond. This fact can be appreciated in the characteristics of the equilibrium configuration, see, α_X bond angle and $d(1,2)$ bond distance. The geometry of the Au-p system at equilibrium is not very different from that observed with a chain of four Au atoms in our previous work where the effect of the tips were neglected.[35]

At the situation of the rupture, (see Table II), all three systems present a linear configuration and the distance of the Au_3-Au_4 bond where it occurs is very similar (~3.1 Å). The contaminated systems arrive to the point of rupture with large Au-Au distances at the Au_1-Au_2 bond; 3.58 Å for the Au-H system and 3.87 Å for the Au-C system. The previous figures indicate that our results are in a very good agreement with the Au-Au separation distances found experimentally[15–21] and with the first-principles calculations from other research groups.[26,32] Up to now, we have only explored the possibility of the incorporation of a single atomic impurity. In relation to this, it must be recognized that the extremely large Au-Au distances of 4–5 Å,[16,25] as well as consecutive distances of 3.5–4 Å (Refs. 15 and 17–20) cannot be reproduced by our calculations. To tackle this point, more impurities should be considered and probably other molecular species as proposed by other groups that performed first-principles calculations.[4,5,16,26,28,29] However, the present approach is not devoted to predict all the Au-Au distances observed, but to understand the effect that an atomic impurity produces on a Au monoatomic NW from energetic, geometrical, electronic, and kinetic viewpoints.

A more detailed information of the behavior of the distances and bond angles of the three systems as the elongation increases can be found in Fig. 3.

In the case of the pure Au system, the four bonds stretch simultaneously up to an average distance of $\bar{d}_{\text{Au-Au}}$ =2.9 Å/atom. At this point, the $d(3,4)$ bond distance starts to increase rapidly, while the other three relax to a value close to the equilibrium one. The contaminated systems show a distinct behavior between each other. The hydrogen atom remains located above the atoms Au_1 and Au_2 up to a chain length of 11 Å ($\bar{d}_{\text{Au-Au}}$=2.75 Å/atom). At this length, this impurity starts to incorporate gradually between the two atoms. On the other hand, the Au-C system appears to be more rigid. Right from the beginning the C atoms appears situated between the Au_1 and Au_2 atoms. In Figs. 3(e) and 3(f) it can be observed that the $d(1,2)$ bond distance and the α_C bond angle remain practically constant upon elongation, showing the remarkable difference between the Au-H and Au-C bonds. In the following, we study the nature of the bonds in the contaminated systems in the light of the analysis of the pseudoelectronic density and the bond order of the atoms involved in pure and contaminated NWs.

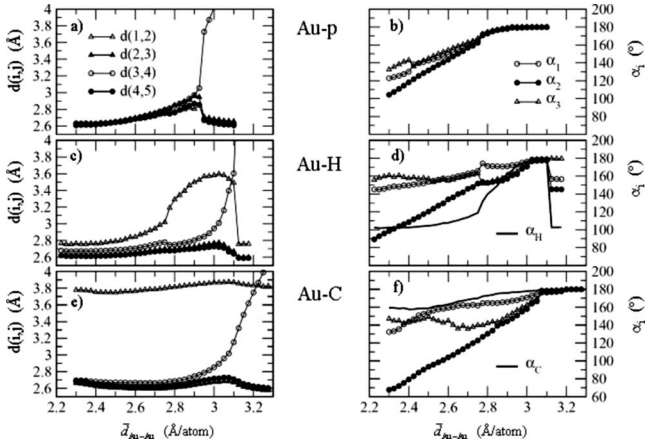

FIG. 3. : Bond distances, $d(i,j)$, and bond angles, α_i, as a function of the Au-Au average separation distance $\bar{d}_{\text{Au-Au}}$ for the systems: (a)–(b) Au-p, (c)–(d) Au-H, and (e)–(f) Au-C.

B. Analysis of the pseudoelectronic density and the bond order in pure and contaminated NWs

Figure 4 shows the differential pseudoelectronic density $\Delta\rho(r)$ of the contaminated NWs for the equilibrium and at rupture conditions. $\Delta\rho(r)$ was calculated from the equation:

$$\Delta\rho(r) = \rho_{\text{Au-X}}(r) - \rho_{\text{Au}}(r) - \rho_X(r), \quad (3)$$

where $\rho_{\text{Au-X}}(r)$ is the pseudoelectronic density of the contaminated system, $\rho_{\text{Au}}(r)$ is the pseudo-electronic density of the system in the absence of the impurity X, and $\rho_X(r)$ is the pseudo-electronic density of the impurity X in the absence of the Au atoms. The plane selected to represent $\Delta\rho(r)$ was the x-z one, which intersects the atoms conforming the atomic NW. The interval considered for $\Delta\rho(r)$ was between −0.05 and 0.08 a.u./bohr^3, with a spacing of de 0.0065 a.u./bohr^3. The structural differences between the Au-H and Au-C systems mentioned above can be easily understood from this plot. The Au-H bond presents no particular directionality, with an electron transfer taking place from Au to H. This resembles the behavior of an ionic bond. On

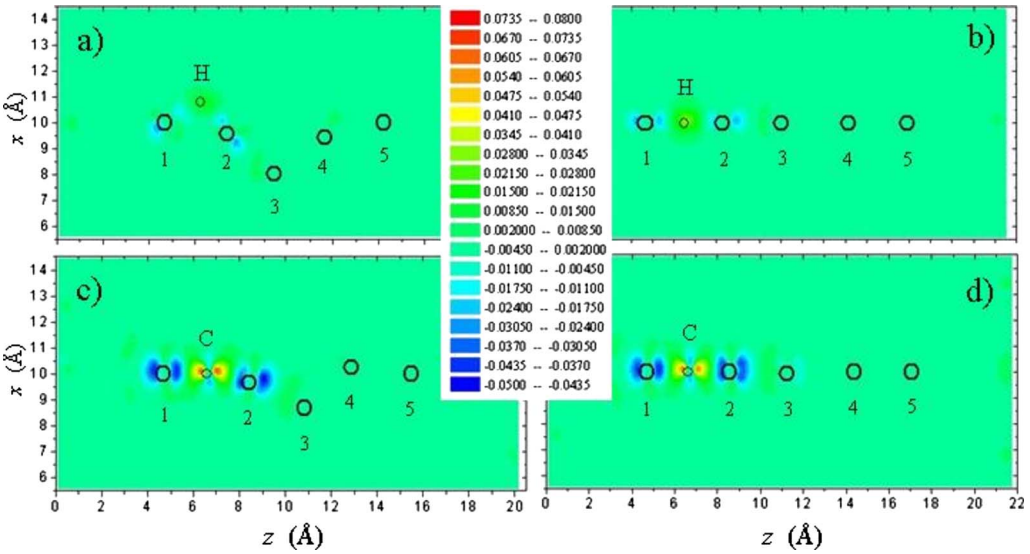

FIG. 4. (Color online) Differential pseudoelectronic density, $\Delta\rho(r)$, for the equilibrium and at rupture geometries of the systems Au-H and Au-C. The big circles indicate the position of the Au atoms, while the small ones denote the atomic impurity. (a) and (c) correspond to $\Delta\rho(r)$ for the equilibrium geometries of the systems Au-H and Au-C respectively. (b) and (d) correspond to $\Delta\rho(r)$ for the at rupture geometry of the systems Au-H y Au-C respectively. The interval considered for $\Delta\rho(r)$ is between -0.05 and 0.08 a.u./bohr^3, with a spacing of 0.0065 a.u./bohr^3. Red and blue correspond to the extreme values of the interval indicating an excess and a depletion of electronic density respectively.

the other hand, the Au-C bond can be interpreted in terms of a covalent interaction, with a marked electronic accumulation between the Au and C atoms. The presence of impurities causes a charge redistribution at the neighboring Au_2-Au_3 bond, making it shorter and less flexible upon elongation with respect to the Au-p system [compare $d(2,3)$ values of Tables I and II]. This is reflected in Fig. 4, where in both systems a net electronic accumulation between the atoms Au_2 and Au_3 occur. This is true for both, the equilibrium and the at rupture geometry. The strengthening of the Au_2-Au_3 bond in the contaminated systems leads to the rupture at the Au_3-Au_4 bond. This bond is longer and more flexible than it analogous in the Au-p system during the whole elongation process, as can be seen in Figs. 3(a) and 3(e).

Another important quantity of common used in theoretical chemistry to analyze bond strength is the so-called "bond order." The bond order between two atoms, say A and B, makes reference to the population of the electrons at the region between A and B forming part of a molecular entity, extracted from the electronic density in this region. There are different ways of partitioning the electronic density, leading to different definitions of the bond order. In the present case, we adopt the scheme derived form the Mülliken population analysis.[48] Here, the bond order is associated to the overlap population between the atoms A and B according to

$$q(\mathrm{A},\mathrm{B}) = \sum_{\mu}^{\mathrm{A}} \sum_{\nu}^{\mathrm{B}} \mathrm{P}_{\mu\nu}\mathrm{S}_{\mu\nu}, \tag{4}$$

where $\mathrm{P}_{\mu\nu}$ and $\mathrm{S}_{\mu\nu}$ are the elements of the density matrix and the overlap matrix respectively. A positive and large value of $q(\mathrm{A},\mathrm{B})$ generally means a strong bond between the atoms A and B, while a negative value implies that the electrons are displaced from the interatomic region by an antibonding interaction.

Figure 5 shows the bond order between the Au atoms as a function of the elongation for the systems under consideration.

The information provided by Fig. 5 is complementary to that of Fig. 4. We clearly see how the Au_2-Au_3 bond becomes strengthened as a consequence of the incorporation of the atomic impurity to the NW. The $q(2,3)$ bond order remains practically constant all over the elongation, with an average value of 0.25 a.u. for the contaminated systems, remarkably larger than that of the Au-p system. We can also observe a strengthening of the Au_4-Au_5 bond and a weakening of the Au_3-Au_4 bond in comparison with Au-p. Figure 5 shows a discontinuity in the $q(3,4)$ bond order of the Au-H system for an average Au-Au distance de 2.75 Å/atom. This is related to the structural change of the Au-H system observed in Figs. 3(c) and 3(d) when the H atom inserts between the atoms Au_1 and Au_2.

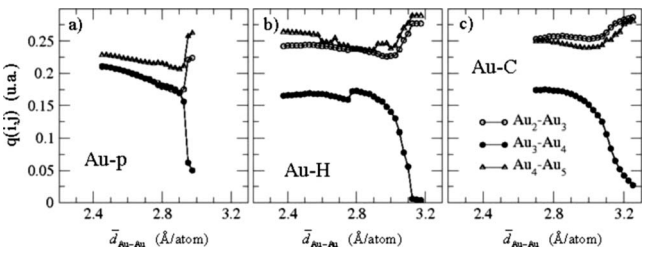

FIG. 5. Bond order, $q(i,j)$, between the i and j Au atoms, as a function of the average Au-Au interatomic distance $\bar{d}_{\mathrm{Au\text{-}Au}}$ for the systems (a) Au-p, (b) Au-H, and (c) Au-C.

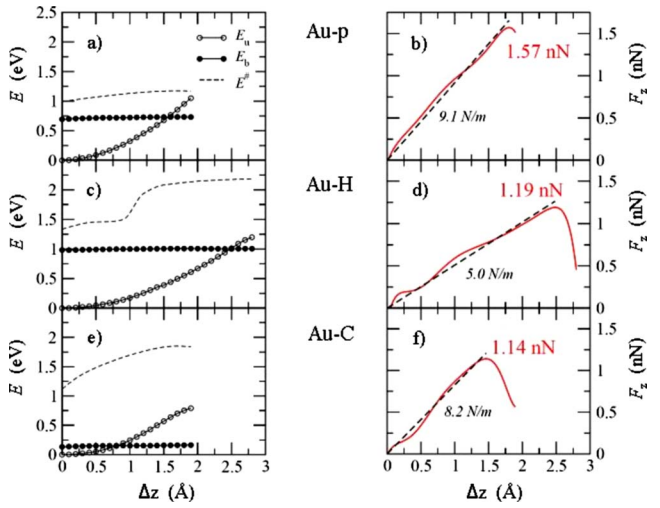

FIG. 6. (Color online) Left: Energy values corresponding to the unbroken state E_u, broken state E_b and activated state $E^{\#}$ of the systems (a) Au-p, (c) Au-H, and (e) Au-C as a function of the elongation Δz. The activation energy for the rupture of the NW at each Δz is $\Delta E^{\neq}=E^{\#}-E_u$. Right, continuous curve: z component of the force acting on the system, F_z, calculated according to Eq. (2), as a function of Δz. The systems considered were (b) Au-p, (d) Au-H, and (f) Au-C. Right, broken line: linear fit to F_z between zero and the maximum force. The maximum force F_z^{max} is indicated in normal typeset, while the force constants, k_z, (slope of the broken lines) are denoted in italics.

C. Analysis of the time stability of pure and contaminated NWs

In the following we consider the kinetic aspects of the rupture process at the Au-p, Au-H and Au-C systems. Inspired in the proposal of Ref. 11, we developed in Ref. 35 a model based on transition state theory (TST) to study the time stability of a monatomic NW and applied it to a model system made of four Au atoms. In short, this model considered for each elongation Δz of a NW three states: an initial state with the unbroken NW (state **u**), a final state with the broken NW (state **b**), and the corresponding transition state (state #) in between. The transition state was calculated using the double nudged elastic band (DNEB) method,[49] associated with the limited memory Broyden-Fletcher-Goldfarb-Shanno (L-BFGS) minimization algorithm.[50] On the average, the DNEB/L-BFGS methodology only required 30 iteration steps to reach convergence in the case of the Au-p system. The Au-H and Au-C systems resulted more demanding computationally, requiring on the average 80 iterations until convergence. Once the activation energy for the reaction path is known, the rates and lifetime of the NW can be calculated straightforwardly using TST. Though its simplicity, satisfactory agreement was found with experimental results[35,51] for the lifetime of a NW. Here, we apply the same model to the Au-p, Au-H, and Au-C systems, using analogous considerations and approximations. Figures 6(a), 6(c), and 6(e) show the energy curves for the unbroken (u), broken (b), and activated (#) states of the Au-p, Au-H, and Au-C systems, respectively, as a function of the elongation Δz. The energy curves of the unbroken state E_u for the three systems correspond to the energy curves shown previously in Fig. 2. In order to find candidate configurations for the broken (final in TST jargon) state at each elongation, molecular dynamic runs were performed at an elongation corresponding to the at rupture configuration. This lead to structures that looked like those illustrated on the broken state (b) configurations of Fig. 8 below. This configuration was then adopted to obtain the broken state for different elongations. This was achieved by compressing the system to a cell size corresponding to the desired L, and then performing a conjugate gradient minimization to obtain the "broken" state for each Δz.

We will perform a more detailed discussion of the reaction path for the rupture of the NWs below. We consider first the behavior of the forces along the stretching procedure, since they are closely related to the energy curves of the unbroken state. In fact, the (u) energy curves of Fig. 6 may be used to calculate the longitudinal force F_z acting on this system according to Eq. (2). In a previous work,[35] we found that the stability limit of a Au monoatomic NW is reached for a force of 1.45 nN. Force experimental measurements of a monatomic Au NW have been undertaken using a combination of a scanning tunneling microscope (STM) and an atomic force microscope (AFM).[47] The maximum experimental force that the wires were found to resist is 1.5 ± 0.3 nN.[18,47,52] Figures 6(b), 6(d), and 6(f) show F_z for the Au-p, Au-H, and Au-C systems respectively, as a function of the elongation Δz. The maximum forces F_z^{max} are also reported there. For the Au-p system, the maximum force is 1.57 nN, in excellent agreement with previous experimental[18,47,52] and theoretical values.[6,35,47] In the case of the contaminated systems, this value is somewhat lower (1.19 nN for Au-H and 1.14 nN for Au-C). First-principles results of literature show the same trend.[26,32]

In their studies of the mechanic properties of monatomic Au NWs, Rubio-Bollinger *et al.*[47] found that these chains are five times harder than the massive electrodes. They evaluated from the experimental results the slopes of the force curves in the last stage of the elastic deformation, before the rupture of the NW, from a set of 200 experiments. The average value of the force constant for an average chain length was 8 N/m. The present calculations show that the behavior of the force curves of the Au-p, Au-H, and Au-C systems is quite elastic, as can be inferred from the linear fit of F_z between zero and the maximum force, shown in Figs. 6(b), 6(d), and 6(f) as broken lines. In the elastic deformation region, the force F_z may be written as:

$$F_z = k_z \Delta z, \tag{5}$$

where k_z is the force constant of the system. The value of k_z found from the present calculations for Au-p, 9.1 N/m, is in perfect agreement with the experimental value reported in Refs. 47 and 53. The contaminated systems present a remarkably different behavior between each other. The Au-C system has $k_z=8.1$ N/m, a very similar value to that of Au-p, but 1.6 larger than the value of this property for Au-H ($k_z=5.0$ N/m). These are interesting predictions, since up to date no measurements have been performed comparing pure and contaminated systems. A suitable fitting of the experimental data of this property could help to shed light on the

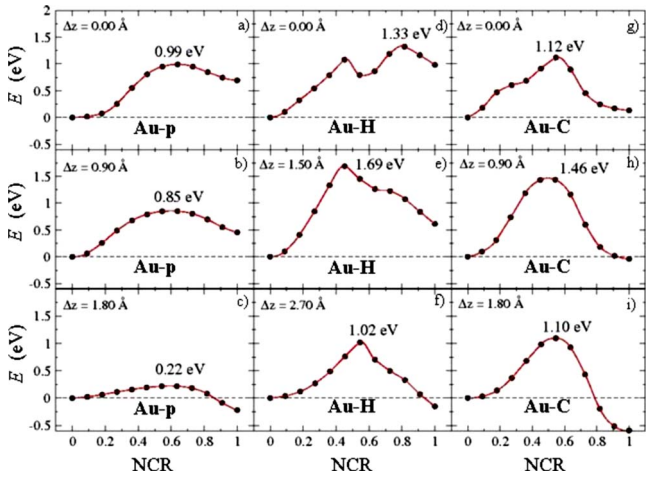

FIG. 7. (Color online) System energy, E, as a function of the NRC along the reaction path between (u) and (b) states for different elongations Δz of the NW. (a)–(c) correspond to the Au-p system, (d)–(f) to the Au-H system, and (g)–(i) to the Au-C system. In all cases the energy of the system is referred to the energy of the (u) state. The activation energies $\Delta E^{\neq}$ and the corresponding elongations are given for each case in the figure.

type of impurity present when a NW exhibits large Au-Au separation distances.

Figure 7 shows the energy of the system, E, as a function of the NRC for the systems analyzed here for some sample elongations. The corresponding configurations are presented in Fig. 8.

Figure 7 shows that the Au-H system presents an energy curve along the minimum energy path that is more complex than those of the Au-p and Au-C systems. At short elongations the energy curves of Au-H present a minimum. This behavior is related to the incorporation of the hydrogen atom into the wire that takes place as the elongation proceeds [see $d(1,2)$ and α_H as a function of $\bar{d}_{\text{Au-Au}}$ for the Au-H system in Fig. 3]. This behavior must be contrasted with that of the Au-C system, where the C atom is incorporated into the wire since the beginning of the elongation [see $d(1,2)$ and α_C as a function of $\bar{d}_{\text{Au-Au}}$ for the Au-C system in Fig. 3]. The minimum in the minimum energy path profile of the Au-H system disappears gradually with increasing elongation of the NW, remaining a shoulder at long elongations. Another relevant feature of Fig. 8 is that the activation energies for the contaminated systems are larger than those of the Au-p system for all elongations studied.

The images of monatomic Au chains showing long separation distances (3.6–4 Å) where obtained by TEM and HR-TEM using electron beam lithography for the fabrication of the NWs.[15–20] Under these experimental conditions, the elongation rate is not controlled and in principle not known. However, an estimation can be made looking at the pictures provided in one of these publications[17] and is found to be very slow, of the order of 0.1 nm/s in the final stage, allowing for a complete equilibration of the system at the atomic scale all along the elongation process. Thus, the rupture of the NWs in these experiments takes place in the time scale of a second, so that in can be inferred that the activation barriers

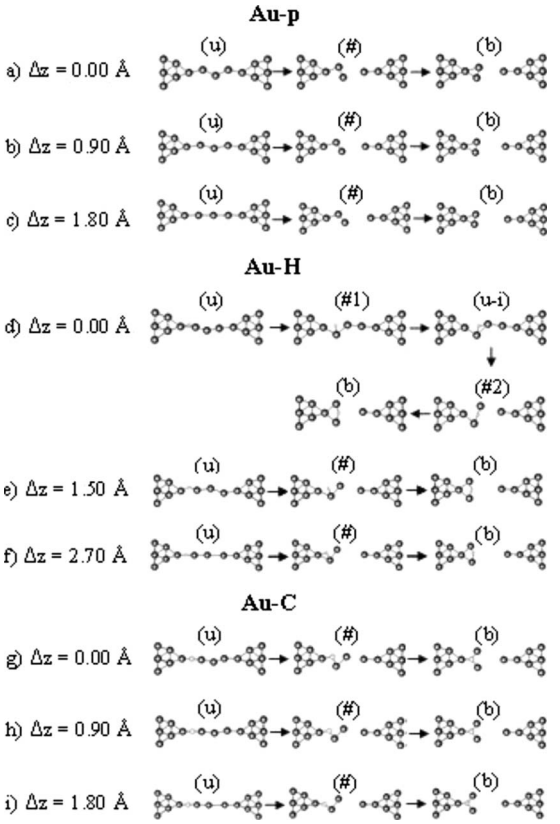

FIG. 8. Configurations of the (u), (#), and (b) states of the NW for each of the elongations Δz whose energy curves along the reaction path are shown in Fig. 7.

must be quite high. In a previous work,[35] we developed a framework to determine the lifetimes of the NWs from the activation energies obtained at different elongations. In the static limit, the lifetime τ^* of a NW can be estimated from:[35]

$$\tau^* = \left[\nu_u(\Delta z) \exp\left(- \frac{\Delta E^{\neq}(\Delta z)}{kT} \right) \right]^{-1}, \tag{6}$$

where $\Delta E^{\neq}(\Delta z)$ is the elongation-dependent activation energy and $\nu_u(\Delta z)$ is a pre-exponential factor that in the case of pure Au NWs was approximated by the longitudinal phonon frequencies of a Au NW.[3] We explain briefly here the reason for this approximation. Within harmonic transition state theory, the pre-exponential factor for the rate constant equation is written as the ratio between the partition functions of the activated complex and the reactants, where numerator and denominator contain vibrational partitions functions of the type $(1-e^{-h\nu/kT})^{-1}$. In the classical limit and when only the most relevant mode with frequency ν_u is considered, the pre-exponencial factor reduces to this frequency ν_u. According to the work of Sánchez-Portal *et al.*,[3] the longitudinal mode of the wire is the one where the frequencies turn negative upon elongation, implying the breaking of the unstable wire along this mode. This vibrational frequency could be employed via a parametrization to approximate the pre-exponential factor of pure nanowires.[35] However, since the results depend only weakly on this factor and we are only seeking for a qualitative comparison between different sys-

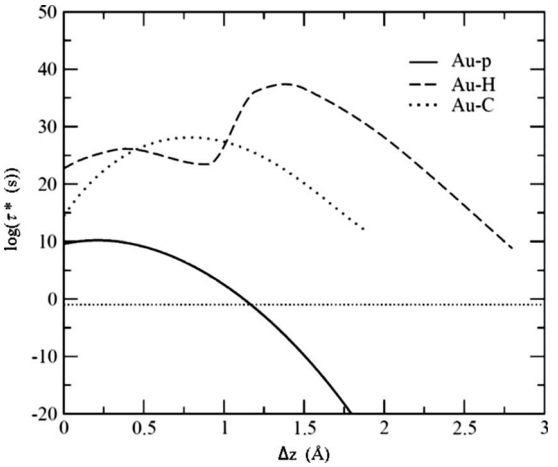

FIG. 9. Decimal logarithm of the lifetimes τ^* of the NWs corresponding to the systems Au-p (—), Au-H (---), and Au-C (· · · ·) as a function of the elongation Δz, calculated according to Eq. (6). The horizontal dotted line denotes a constant lifetime of 0.1 s.

tems, we have used overall $\upsilon_u(\Delta z)=\upsilon_u=3.5\times10^{12}$ Hz and $T=300$ K. Similar values were used in Refs. 35, 52, 54, and 55.

Figure 9 shows a plot of the decimal logarithm of the lifetime τ^* of the NW, calculated from Eq. (6), as a function of the elongation Δz for the Au-p, Au-H, and Au-C systems. It becomes evident from this figure that the contaminated NWs live considerably longer than Au-p NWs for all elongations. This plot also shows that pure Au NWs become unstable in the experimental time scale from $\Delta z=1.17$ Å on, which corresponds to $\bar{d}_{\text{Au-Au}}=2.74$ Å/atom. In fact, for larger Δz ($\bar{d}_{\text{Au-Au}}$), pure NWs should live less than 0.1 s. The remarkable behavior of the Au-H system is due to the shape of the activation energy, discussed above in Fig. 7. Figure 9 also supports the idea that impurities are responsible for the large Au-Au distances observed experimentally. These impurities, as stated above, modify geometrically the structure of the NWs, giving place to the occurrence of the anomalous large Au-Au distances. Furthermore, they modify the NW chemically by charge transfer and rearrangement, which in turn change the potential energy surfaces so that for each elongation the contaminated NWs present higher activation barriers for the ruptures than the Au-p NWs. Figure 9 makes also plausible that stretched (contaminated) NWs may have lifetimes of the order of the second, sometimes even of the order of minutes.[15]

D. Analysis of reaction force and transition region

As we saw in the previous section, the contaminated systems present larger activation barriers that Au-p along the reaction coordinate. However, it is at first sight puzzling that the three systems studied break at the same bond, Au_3-Au_4, with similar rupture forces, which appear to be smaller in the case of the contaminated systems. On the other hand, the force constant k_z of the Au-H system indicates that this system is relatively soft in comparison with the Au-p and Au-C systems. So, how is a larger activation energy for the rupture

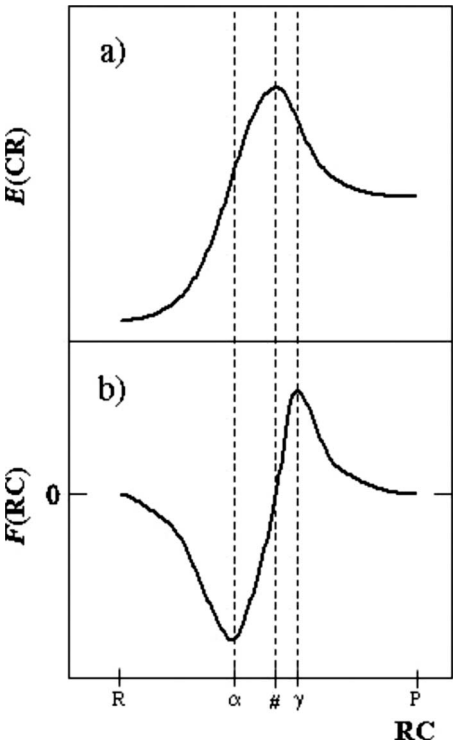

FIG. 10. (a) Potential energy of the system, E(RC), and (b) and reaction force, F(RC), as a function of the RC for a generic elementary process.

compatible with a seemingly softer bond? The key to understand this apparent discrepancy is that the force that we are calculating corresponds to the stretching in one direction of the system (axis z), that is, the longitudinal direction of the NW, while the motion along the reaction coordinate is not necessarily in this direction. For this reason, to gain further insight into the chemical aspects of the rupture process of the NWs, we will address ourselves to the concept of reaction force as developed by Toro Labbé and co-workers.[36,37]

1. Reaction force definition

The concept of reaction force F(RC) is based on the classical expression of force as the negative gradient of the potential energy of the system under consideration. For a chemical or physical process it is defined as

$$F(\text{RC}) = -\frac{\partial E(\text{RC})}{\partial \text{RC}}, \tag{7}$$

where E(RC) is the potential energy of the system along the RC running from reactants to products. As we have already seen, for an elementary process, E(RC) has a shape similar to that shown in Fig. 10(a). According to Eq. (7), F(CR) presents a minimum and a maximum at the inflection points of E(RC), one at RC$=\alpha$ and another one at RC$=\gamma$. Figure 10(b) depicts schematically F(RC) as a function of RC, showing a partition of the reaction path in three regions: (1) reactants (R)$\rightarrow\alpha$, (2) intermediate $\alpha\rightarrow\gamma$, and (3) products $\gamma\rightarrow$(P).

Within this partition, it is generally found that in the first region, (R)$\rightarrow\alpha$, previous to the minimum of F(RC), struc-

tural changes in the reactants take place. These are related to compression and elongation of bonds, torsion of angles, etc. This is the elastic or harmonic stage of the process. The resistance to these changes leads to an increasing negative force that tries to reconstitute the reactants. This reconstitutive force reaches its maximum absolute value at RC=α. This is an important point, since it can be stated that the system has reached an "activated state" for the reactants to be driven into products. The second region extends from the minimum of F(RC) at α up to its maximum at γ. In this region, the largest changes driving the reactants into products take place. The most extensive changes in the electronic properties of the system occur here (changes in the electrostatic potential, the density of states, the reaction order, the ionization energies, etc.), with the concomitant creation (rupture) of chemical bonds. These changes lead to an increasing positive force that starts to be evident at α and gradually overcomes the reconstitutive force of the previous region. Both forces are exactly equal in magnitude and perfectly balanced at RC=#. After this point, the positive force is dominant and monotonically increasing up to RC=γ. In the last region, for RC$>\gamma$, structural relaxations take place that drive the system toward the final state of products (P). An important aspect of the reaction force analysis, as proposed by Toro Labbé and co-workers,[36,37] is the natural decomposition of the activation energy $\Delta E^{\neq}$ into two components. To achieve this, we note that in the present notation we have

$$\Delta E^{\neq} = E(\#) - E(\mathrm{R}), \tag{8}$$

where $E(\#)$ is the energy of the activated state and is the energy of the reactants E(R). Through addition and subtraction of the energy of the system at point α, $E(\alpha)$, on the right-hand side we get

$$\Delta E^{\neq} = [E(\#) - E(\alpha)] + [E(\alpha) - E(\mathrm{R})] = \Delta E_2^{\neq} + \Delta E_1^{\neq}, \tag{9}$$

where $\Delta E_2^{\neq}$ and $\Delta E_1^{\neq}$ correspond to the first and second parenthesis at the center of Eq. (9), respectively. According to this definition, $\Delta E_1^{\neq}$ is the activation energy required in the first region, (R)$\rightarrow\alpha$, to overcome the early structural changes of the system. It is a configurational energy change, in the sense that in can be formally predicted from the structure of the system assuming an elastic behavior. On the other hand, $\Delta E_2^{\neq}$ is the energy required in the $\alpha\rightarrow\gamma$ region to change the electronic properties of the system to take it up to the activated state (#). For this reason, we will refer to it as an electronic energy contribution.

2. Reaction force in pure and contaminated NWs

The concept of reaction force stated above was applied to the Au-p, Au-H, and Au-C systems for a chain length L of 11.2 Å, where the Au-Au average separation distance was $\bar{d}_{\text{Au-Au}}$=2.8 Å. Figure 11 shows the behavior of E(RC) and F(RC) for the different systems for this chain length. Analogously to the previous discussion, it is possible to distinguish three regions along the reaction coordinate: (i) unbroken region (u)$\rightarrow\alpha$, (ii) transition region $\alpha\rightarrow\gamma$, and (iii) broken region $\gamma\rightarrow$(b). As done previously in Fig. 7, the energy of the system, E(RC), was referred to that of the unbroken wire, so that the activation energy $\Delta E^{\neq}$ and the components $\Delta E_1^{\neq}$ and $\Delta E_2^{\neq}$ defined in Eq. (9) take the following form

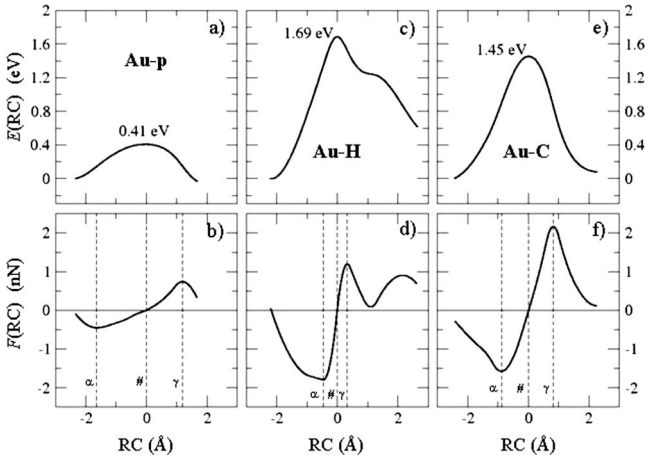

FIG. 11. System energy, E(RC), and reaction force, F(RC), as a function of the reaction coordinate (RC) for the systems Au-p (a) and (b), Au-H (c) and d), and Au-C (e) and (f) for a chain length $L\cong$11.2 Å ($\bar{d}_{\text{Au-Au}}$=2.8 Å). The vertical broken lines in (b), (d), and (f) denote RC=α, RC=#, and RC=γ.

$$\Delta E^{\neq} = E(\#),$$

$$\Delta E_1^{\neq} = E(\alpha),$$

$$\Delta E_2^{\neq} = \Delta E^{\neq} - E(\alpha). \tag{10}$$

In the particular case of the Au-H system, F(RC) shows in Fig. 11 a somewhat more complex behavior in the $\gamma\rightarrow$(b) region than that expected from the considerations made with Fig. 10. This is due to the presence of the shoulder in the corresponding E(RC) curves. This has no consequences for the following force analysis, since it is concerned with the (u)$\rightarrow$# region.

Comparison of the three systems considered in Fig. 11, shows that in the (u)$\rightarrow\alpha$ region the reaction force in remarkably more negative for the contaminated systems than for Au-p. The force at the point α, $F(\alpha)$, which characterizes a situation where the system has definitely abandoned an elastic behavior can be interpreted as a rupture force in the direction of the reaction coordinate. This quantity is more suited to compare the behavior of the different systems than the force $F_z^{\max}$ addressed above. In fact, while $F(\alpha)$ operates along the reaction coordinate and corresponds to the spontaneous (thermal) rupture of the NW at a given elongation, the force $F_z^{\max}$ relates to the rupture of the system driven by its stretching. The latter would be only meaningful if the stretching would be undertaken in the limit $T\rightarrow 0$, where thermal fluctuations do not play any role in the rupture process and the system would break due to straightforward application of an external force.

The absolute value of $F(\alpha)$, together with the force F_z for $\bar{d}_{\text{Au-Au}}$=2.8 Å, are compiled in Table III for the three system. Considering the static rupture of the NW, as it occurs in the electron beam lithography experiments,[15–20] we must re-

TABLE III. Quantitative information as obtained from the results of Fig. 12. Force in the direction of the elongation, F_z, calculated according to Eq. (2). Absolute value of the reaction force, $F(\alpha)$, at the α point. Activation energy $\Delta E^{\neq}$ and its components $\Delta E_1^{\neq}$ and $\Delta E_2^{\neq}$ for the systems Au-p, Au-H, and Au-C for a chain length $L \cong 11.2$ Å ($\bar{d}_{\text{Au-Au}}=2.8$ Å). The maximum force values, $F_z^{\max}$, of Fig. 6 are included for comparison.

	Au-p	Au-H	Au-C
F_Z(nN)	1.40	0.80	0.40
$\lvert F(\alpha)\rvert$(nN)	0.44	1.80	1.58
$F_Z^{\max}$(nN)	1.57	1.19	1.14
$\Delta E^{\neq}$(eV)	0.41	1.69	1.45
$\Delta E_1^{\neq}$(eV)	0.14	1.34	0.91
$\Delta E_2^{\neq}$(eV)	0.27	0.35	0.54

member that this process occur mainly via thermal fluctuations. The relatively low $\lvert F(\alpha)\rvert$ of the Au-p (0.44 nN) clearly indicates that these systems will be less stable than the contaminated ones. This conclusion could not be drawn from the $F_z^{\max}$, also included in Table III for comparison.

Another interesting point to note in Fig. 11 is the larger extension of the (u)$\rightarrow\alpha$ region in the case of the contaminated wires. This means that these systems are more flexible than the pure nanowire, in the sense that a longer path must be gone along the RC in order to reach the region where elastic behavior is definitively abandoned. We will come back again below on the reasons for this behavior.

The area under the curve F(RC) in the (u)$\rightarrow\alpha$ region is the energy change $\Delta E_1^{\neq}$, while that in the $\alpha\rightarrow$# region is the energy change $\Delta E_2^{\neq}$. These quantities are also reported in Table III. It can be observed that the electronic contribution, $\Delta E_2^{\neq}$, is similar in all cases. On the opposite, pure and contaminated systems present strong differences in the configurational contribution $\Delta E_1^{\neq}$. It can be thus concluded that in the case of the contaminated systems, the main hindrance to cross the barrier between the (u) and (b) states is in the (u) $\rightarrow\alpha$ region, where the structural changes preparing the system for the activated state occur.

The bond order defined in Sec. III B is a relevant electronic property of the system. This quantity, according to the concept of reaction force, should present its largest changes in the $\alpha\rightarrow\gamma$ transition region, as proposed by Herrera *et al.* in Ref. 56. Figure 12 shows the behavior of the q(i,j) bond order between atoms i and j along the reaction path for the Au-p, Au-H and Au-C systems for a chain length $L \cong 11.2$ Å. There, the additional bond (Au_1-Au_3) is considered because its appearance during the reaction course. For the contaminated systems, the largest changes of q(i,j) in the $\alpha\rightarrow\gamma$ transition region are found at the Au_2-Au_3 bond.

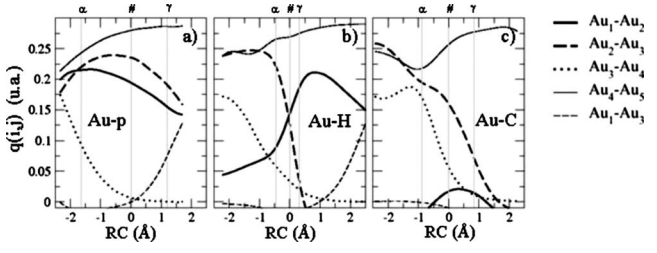

FIG. 12. Bond order, q(i,j), between the atoms Au_i and Au_j as a function of the reaction coordinate RC of the systems (a) Au-p, (b) Au-H, and (c) Au-C for the chain length $L \cong 11.2$ Å.

The $q(3,4)$ bond order of the Au-C system also changes considerably in this region, at variance with the Au-H system, where the strongest change in $q(3,4)$ is found in the (u)$\rightarrow\alpha$ region. In the case of the Au-p system, the strongest changes are noticed at $q(3,4)$, especially at the transition $\alpha\rightarrow\gamma$ region. We can conclude that the energy contribution $\Delta E_2^{\neq}$ of the contaminated systems is used essentially to the subtraction of electron density from the Au_2-Au_3 bond, thus decreasing $q(2,3)$. We must point out that at the equilibrium state the H and C impurities considerably reinforce its neighboring bond, in the present case the Au_2-Au_3 one [note the larger value of $q(2,3)$ at low RC in the case of Au-H and Au-C with respect to Au-p, Fig. 12]. As we pointed above, the region (u)$\rightarrow\alpha$ is more extended in the case of the contaminated wires. It is remarkable that in this region, $q(3,4)$ shows in these cases an arrest that is absent in the case Au-p. This fact, along with the larger $q(2,3)$ values suggest that the impurities are buffering the bond order of the neighboring Au-Au bonds upon elongation of the system. This buffering is particularly important at the initial part of RC and is responsible for the larger extension of the (u)$\rightarrow\alpha$ region in the case of the contaminated wires.

IV. CONCLUSIONS

We have analyzed the energetic and kinetic stability of pure and contaminated Au nanowires. In the latter case, we considered the presence of H and C impurities under different elongations of the nanowire. In the case of the contaminated NWs, the Au-Au distances calculated agree with experimental values of Refs. 15–20.

The stability of the contaminated nanowires is due to important charge redistribution at the nanowires due to the presence of the impurities. At the equilibrium state, an important strengthening is observed at the Au-Au bond neighboring the impurity, as well as a weakening of the second nearest bond to the impurity. This insertion occurs in the case of C practically from the beginning, while in the case of H it takes place in a progressive fashion.

The kinetics of the rupture process was investigated for pure Au nanowires, as well as for their analogous contaminated with H and C. The latter present larger activation energies for the rupture for all elongations, and as a consequence this wires live longer, as observed experimentally.

The concept of reaction force was applied to the present problem, showing that this is the relevant quantity to analyze when considering the stability of the nanowires in the limit of slow elongations rates or relatively high temperatures, rather than the longitudinal force acting on the nanowire. This analysis was used to shed light on the elastic and electronic contributions to the rupture process. While the latter are similar in all cases, the elastic part plays the decisive role to make the difference. Bond order analysis suggests that the enhanced elastic behavior of contaminated nanowires is due

to a buffering effect of impurities on the bond order of the Au-Au bond directly involved in the rupture.

We think that the present modeling may be useful to analyze the possibility of contamination by other atoms, suggesting that measurement of the force constant of the junction may help to determine the chemical nature of the impurity.

ACKNOWLEDGMENTS

Financial support from CONICET, Secyt UNC, and Program BID 1728/OC-AR PICT No. 946 are gratefully acknowledged. P.V. thanks CONICET.

*Corresponding author; eze_leiva@yahoo.com.ar

[1] M. Okamoto and K. Takayanagi, Phys. Rev. B **60**, 7808 (1999).
[2] J. Nakamura, N. Kobayashi, and M. Aono, RIKEN Rev. **37**, 17 (2001).
[3] D. Sánchez-Portal, E. Artacho, J. Junquera, P. Ordejón, A. García, and J. M. Soler, Phys. Rev. Lett. **83**, 3884 (1999).
[4] S. R. Bahn, N. López, J. K. Nørskov, and K. W. Jacobsen, Phys. Rev. B **66**, 081405(R) (2002).
[5] N. V. Skorodumova and S. I. Simak, Phys. Rev. B **67**, 121404(R) (2003).
[6] E. Z. da Silva, F. D. Novaes, A. J. R. da Silva, and A. Fazzio, Phys. Rev. B **69**, 115411 (2004).
[7] L. De Maria and M. Springborg, Chem. Phys. Lett. **323**, 293 (2000).
[8] H. Häkkinen, R. N. Barnett, A. G. Scherbakov, and U. Landman, J. Phys. Chem. B **104**, 9063 (2000).
[9] W. T. Geng and K. S. Kim, Phys. Rev. B **67**, 233403 (2003).
[10] N. V. Skorodumova, S. I. Simak, A. E. Kochetov, and B. Johansson, Phys. Rev. B **72**, 193413 (2005).
[11] L. Ke, T. Kotani, M. van Schilfgaarde, and P. A. Bennett, Nanotechnology **18**, 424002 (2007).
[12] P. Jelínek, R. Pérez, J. Ortega, and F. Flores, Phys. Rev. B **77**, 115447 (2008).
[13] E. Z. da Silva, A. J. R. da Silva, and A. Fazzio, Phys. Rev. Lett. **87**, 256102 (2001).
[14] M. Dreher, F. Pauly, J. Heurich, J. C. Cuevas, E. Scheer, and P. Nielaba, Phys. Rev. B **72**, 075435 (2005).
[15] H. Ohnishi, Y. Kondo, and K. Takayanagi, Nature (London) **395**, 780 (1998).
[16] S. B. Legoas, D. S. Galvao, V. Rodrigues, and D. Ugarte, Phys. Rev. Lett. **88**, 076105 (2002).
[17] V. Rodrigues and D. Ugarte, Phys. Rev. B **63**, 073405 (2001).
[18] T. Kizuka, Phys. Rev. B **77**, 155401 (2008).
[19] V. Rodrigues, T. Fuhrer, and D. Ugarte, Phys. Rev. Lett. **85**, 4124 (2000).
[20] Y. Kondo and K. Takayanagi, Science **289**, 606 (2000).
[21] A. I. Yanson, G. Rubio Bollinger, H. E. van den Brom, N. Agrait, and J. M. van Ruitenbeek, Nature (London) **395**, 783 (1998).
[22] Y. Takai, T. Kawasaki, Y. Kimura, T. Ikuta, and R. Shimizu, Phys. Rev. Lett. **87**, 106105 (2001).
[23] J. F. O'Hanlon, *A User's Guide to Vacuum Technology* (Wiley, New York, 1989).
[24] S. B. Legoas, V. Rodrigues, D. Ugarte, and D. S. Galvão, Phys. Rev. Lett. **93**, 216103 (2004).
[25] H. Koizumi, Y. Oshima, Y. Kondo and K. Takayanagui, Ultramicroscopy **88**, 17 (2001).
[26] F. D. Novaes, A. J. R. da Silva, E. Z. da Silva, and A. Fazzio, Phys. Rev. Lett. **90**, 036101 (2003).
[27] F. D. Novaes, A. J. R. da Silva, E. Z. da Silva, and A. Fazzio, Phys. Rev. Lett. **96**, 016104 (2006).
[28] D. S. Galvão, V. Rodríguez, D. Ugarte, and S. B. Legoas, Mater. Res. **7**, 339 (2004).
[29] N. V. Skorodumova and S. I. Simak, Solid State Commun. **130**, 755 (2004).
[30] E. Hobi, A. J. R. da Silva, F. D. Novaes, E. Z. da Silva, and A. Fazzio, Phys. Rev. Lett. **95**, 169601 (2005).
[31] S. B. Lagoas, V. Rodrigues, D. Ugarte, and D. S. Galvão, Phys. Rev. Lett. **95**, 169602 (2005).
[32] N. V. Skorodumova, S. I. Simak, A. E. Kochetov, and B. Johansson, Phys. Rev. B **75**, 235440 (2007).
[33] E. Anglada, J. A. Torres, F. Yndurain, and J. M. Soler, Phys. Rev. Lett. **98**, 096102 (2007).
[34] E. Hobi, Jr., A. Fazzio, and A. J. R. da Silva, Phys. Rev. Lett. **100**, 056104 (2008).
[35] P. Vélez, S. A. Dassie, and E. P. M. Leiva, Chem. Phys. Lett. **460**, 261 (2008).
[36] P. Politzer, A. Toro-Labbé, S. Gutiérrez-Oliva, B. Herrera, P. Jaque, M. C. Concha, and J. S. Murria, J. Chem. Sci. **117**, 467 (2005).
[37] A. Toro-Labbé, S. Gutiérrez-Oliva, J. S. Murray, and P. Politzer, J. Mol. Model. **15**, 707 (2009).
[38] G. Henkelman and H. Jónsson, J. Chem. Phys. **113**, 9978 (2000).
[39] G. Henkelman, B. P. Uberuaga, and H. Jónsson, J. Chem. Phys. **113**, 9901 (2000).
[40] P. Ordejón, E. Artacho, and J. M. Soler, Phys. Rev. B **53**, R10441 (1996).
[41] D. Sáchez-Portal, P. Ordejón, and E. Artacho, Int. J. Quantum Chem. **65**, 453 (1997).
[42] E. Artacho, D. Sánchez-Portal, P. Ordejón, A. García, and J. M. Soler, Phys. Status Solidi **215**, 809 (1999).
[43] P. Ordejón, D. Sánchez-Portal, A. García, E. Artacho, J. Junquera, and J. M. Soler, RIKEN Rev. **29**, 42 (2000).
[44] J. M. Soler, E. Artacho, J. D. Gale, A. García, J. Junquera, P. Ordejón, and D. Sánchez-Portal, J. Phys.: Condens. Matter **14**, 2745 (2002).
[45] J. P. Perdew, K. Burke, and M. Ernzerhof, Phys. Rev. Lett. **77**, 3865 (1996).
[46] P. Vélez, S. A. Dassie, and E. P. M. Leiva, Phys. Rev. Lett. **95**, 045503 (2005).
[47] G. Rubio-Bollinger, S. R. Bahn, N. Agraït, K. W. Jacobsen, and S. Vieira, Phys. Rev. Lett. **87**, 026101 (2001).
[48] A. Szabo and N. Ostlund, *Modern Quantum Chemistry* (McGraw-Hill, New York, 1989).
[49] S. A. Trygubenko and D. Wales, J. Chem. Phys. **120**, 2082 (2004).

[50] D. C. Liu and J. Nocedal, Math. Program. **45**, 503 (1989).
[51] Z. Huang, F. Chen, P. A. Bennett, and N. J. Tao, J. Am. Chem. Soc. **129**, 13225 (2007).
[52] G. Rubio, N. Agraït, and S. Vieira, Phys. Rev. Lett. **76**, 2302 (1996).
[53] B. Xu, X. Xiao, and N. J. Tao, J. Am. Chem. Soc. **125**, 16164 (2003).
[54] T. N. Todorov, J. Hoekstra, and A. P. Sutton, Phys. Rev. Lett. **86**, 3606 (2001).
[55] J. Bürki, C. A. Stafford, and D. L. Stein, Phys. Rev. Lett. **95**, 090601 (2005).
[56] B. Herrera and A. Toro-Labbé, J. Chem. Phys. **121**, 7096 (2004).